Chinese Physics Letters

EXPRESS LETTER

Ultrafast Melting of Charge-Density-Wave Order and a Transient Metastable State in $4H_b$-TaS_2

Cite as: Lingxiao Gu *et al*. 2026 *Chin. Phys. Lett.* **43** 090707

DOI CSTR

Recommended Articles

Revealing Light-Induced Charge Density Wave Melting and Carrier Redistribution in 1T-$TiSe_2$

Wanying Chen, Haoyuan Zhong, Changhua Bao, Fei Wang, Xuanxi Cai, Chenxia Yun, Hao Teng, Zhiyi Wei, and Shuyun Zhou
Chin. Phys. Lett. **42**, 017101 (2025)

Tuning the Charge Density Wave and Low-Energy Magnetic States with Nanoscale Strains in $GdTe_3$

Zhong-Yi Cao, Hui Chen, Guo-Jian Qian, Yan-Hao Shi, Qi Qi, Xiang-He Han, Hai-Tao Yang, and Hong-Jun Gao
Chin. Phys. Lett. **42**, 100702 (2025)

Interplay of Charge Density Wave and Magnetism on the Kagomé Lattice

Yu-Han Lin, Jin-Wei Dong, Ruiqing Fu, Xianxin Wu, Ziqiang Wang, and Sen Zhou
Chin. Phys. Lett. **42**, 080709 (2025)

Charge Density Wave Induced Second-Harmonic Generation in 1T-$TaSe_2$

Zhao-Zhe Chen, Chang-Hua Li, Hai-Xia Zhu, Yan-Peng Qi, and Si Xiao
Chin. Phys. Lett. , (2026)

Interplay Between Charge Ordering and Isospin Polarization in hBN-Aligned Twisted Monolayer–Bilayer Graphene

Wang Zhu, Junwei Song, Yajuan Zhao, Kenji Watanabe, Takashi Taniguchi, Haolin Wang, and Lei Wang
Chin. Phys. Lett. , (2026)

Three-Dimensional van Hove Singularities and Charge Density Wave Evolution in Kagome Lattice KV_3Sb_5

Yu Huang *et al*.
Chin. Phys. Lett. **42**, 120704 (2025)

A series journal of Chinese Physical Society distributed by IOP Publishing

Chinese Physics Letters

Chin. Phys. Lett. **43** 090707 (2026)

EXPRESS LETTER

DOI: 10.1088/0256-307X/43/9/090707
CSTR: 32039.14.0256-307X.43.9.090707

Ultrafast Melting of Charge-Density-Wave Order and a Transient Metastable State in $4H_b$-TaS_2

Lingxiao Gu(顾凌霄)[1,2], Fanyu Meng(孟凡玉)[3,4], Wenxuan Yang(杨文轩)[1,2], Shichong Wang(王石崇)[1,2], Haoran Liu(刘浩然)[1,2], Jiongyu Huang(黄炯谕)[1,2], Jianzhe Liu(刘见喆)[1,2], Donghua Chen(陈东华)[2], Shaofeng Duan(段绍峰)[2], Dong Qian(钱冬)[1,5,6], Hechang Lei(雷和畅)[3,4,*], and Wentao Zhang(张文涛)[2,1,*]

[1]Key Laboratory of Artificial Structures and Quantum Control (Ministry of Education), School of Physics and Astronomy, Shanghai Jiao Tong University, Shanghai 200240, China
[2]Beijing National Laboratory for Condensed Matter Physics, Institute of Physics, Chinese Academy of Sciences, Beijing 100190, China
[3]Department of Physics, Beijing Key Laboratory of Optoelectronic Functional Materials & Micro-Nano Devices, Renmin University of China, Beijing 100872, China
[4]Key Laboratory of Quantum State Construction and Manipulation (Ministry of Education), Renmin University of China, Beijing 100872, China
[5]Collaborative Innovation Center of Advanced Microstructures, Nanjing University, Nanjing 210093, China
[6]Tsung-Dao Lee Institute, Shanghai Jiao Tong University, Shanghai 201210, China

*Corresponding authors. Email: hlei@ruc.edu.cn; wentaozhang@iphy.ac.cn

$4H_b$-TaS_2 is a natural heterostructure of correlated (T) and superconducting (H) layers. Using time- and angle-resolved photoemission spectroscopy, we observe a narrow feature slightly above the Fermi level on the T-layer termination, corresponding to the band edge of a charge-density-wave (CDW)-gapped electron-like dispersion. Above a characteristic incident fluence, the fitted CDW gap becomes indistinguishable from zero, while enhanced occupied-state spectral weight persists for tens of picoseconds after hot carriers decay. Together, these spectral and dynamical signatures identify a transient metastable electronic state. Its much shorter lifetime than that of the persistent hidden state in bulk 1T-TaS_2 is consistent with a role for interrupted direct T–T stacking, although relaxation channels involving the H layers may also contribute. These results highlight the influence of the interlayer environment on nonequilibrium-state stability and establish $4H_b$-TaS_2 as a platform for ultrafast control of correlated states.

Ultrafast photoexcitation has emerged as a powerful route to manipulate quantum materials and access transient states that are inaccessible in equilibrium [1,2]. In parallel, van der Waals heterostructures provide a complementary means of control, since proximity effects and interlayer coupling can strongly reshape the electronic structure and collective behavior of their constituent layers [3,4]. Combining ultrafast optical excitation with such interlayer effects offers a promising strategy for engineering emergent nonequilibrium phases. The natural van der Waals heterostructure $4H_b$-TaS_2, composed of alternating layers of correlated 1T-TaS_2 (T) and superconducting 1H-TaS_2 (H) [5,6], provides an ideal platform to explore this interplay. It hosts multiple ordered phases, including two charge-density-wave (CDW) transitions—at 315 K associated with the T layers and at 22 K originating from the H layers—followed by a superconducting transition near 3 K [7–10]. A variety of unconventional phenomena, ranging from chiral superconductivity to putative topological states, have been reported in this material and are often attributed to the interplay between its constituent layers [11–15].

A defining feature of the 1T-TaS_2 layer is the commensurate CDW, which reconstructs the lattice into a $\sqrt{13}\times\sqrt{13}$ superlattice of Star-of-David (SOD) clusters [Fig. 1(a)]. Within each SOD cluster, twelve of the thirteen Ta 5d electrons form bonding molecular orbitals, leaving a single electron per cluster to occupy a narrow, half-filled electronic band [16]. Experimentally, however, such a narrow half-filled band is absent at the Fermi level in both monolayer and bulk 1T-TaS_2. This discrepancy is commonly attributed to correlation effects that open a Mott-like gap, as well as to interlayer dimerization [17,18]. Remarkably, when the CDW order in bulk 1T-TaS_2 is transiently melted by optical or electrical excitation, the system can be driven into a long-lived hidden metallic state whose stability is believed to rely on a particular interlayer stacking order [19–21]. In $4H_b$-TaS_2, intervening H layers interrupt direct T-layer stacking and therefore provide a natural setting to test the role of interlayer coupling in stabilizing such nonequilibrium phases. Previous angle-resolved photoemission spectroscopy (ARPES) and scanning tunneling microscopy (STM) studies have pointed to a CDW-related near-E_F feature on the T-layer termination [22–26], but its dispersion and nonequilibrium dynamics remain unexplored. In particular, it is still unknown whether a photoinduced metastable state analogous to the hidden state in bulk 1T-TaS_2 can be stabilized in $4H_b$-TaS_2, where the interlayer stacking order of T layers is intrinsically disrupted.

In this Letter, we use time- and angle-resolved photoemission spectroscopy (TRARPES) to probe the unoccupied electronic structure and ultrafast dynamics of $4H_b$-TaS_2. We identify a CDW-related band-edge feature near the Fermi level (E_F) on the T-layer termination and track its photoinduced evolution. Our measurements reveal ultrafast suppression of the CDW order, with dynamics consistent with a displacive lattice response. During the subsequent recovery, the system develops a transient metastable electronic state with enhanced occupied-state spectral weight below E_F. This state persists for only tens of picoseconds. Its lifetime contrast with the persistent hidden state in bulk 1T-TaS_2 is consistent with a role for the absence of direct T–T stacking, while possible electronic and phononic relaxation channels involving the intervening H layers cannot be excluded.

Ultrafast electronic-structure measurements were performed using a home-built TRARPES system with overall energy and temporal resolutions of approximately 16.3 meV and 113 fs, respectively [27,28]. The samples were photoexcited by infrared pump pulses centered at 700 nm ($h\nu = 1.77$ eV) and probed by ultraviolet pulses at 205 nm ($h\nu = 6.05$ eV). To minimize cumulative laser heating, the pump laser was operated at a repetition rate of 125 kHz. The pump and probe spot sizes were approximately 80 μm and 20 μm, respectively. The quoted pump fluences are peak incident fluences; no correction for optical reflectivity or absorption was applied. Equilibrium ARPES

Received 23 July 2026; accepted 18 August 2026; published 2 September 2026
© 2026 Chinese Physical Society and IOP Publishing Ltd. All rights, including for text and data mining, AI training, and similar technologies, are reserved.

Check for updates

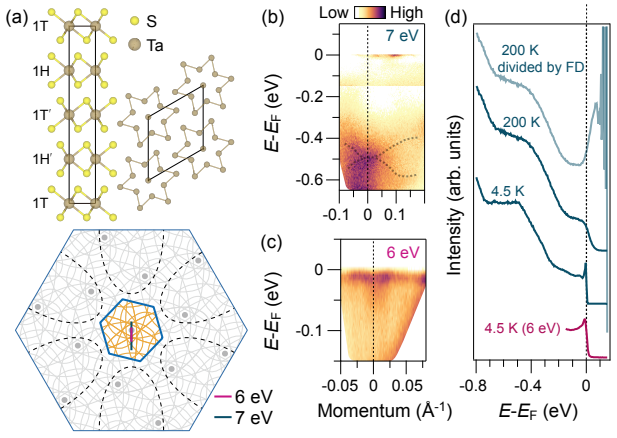

Fig. 1. Equilibrium ARPES spectra of $4H_b$-TaS_2 near the BZ center along the Γ–M direction. (a) Crystal structure, SOD cluster reconstruction in the T layer, and superlattice-induced band folding in the BZ. Dashed and solid lines schematically indicate the bands in the normal phase and the folded bands in the CDW state, respectively. (b) and (c) Spectra measured at 4.5 K with photon energies of 7 eV and 6 eV, respectively; dashed lines guide the eye to the dispersive features near −0.5 eV. (d) Momentum-integrated EDCs around the Γ point measured at 4.5 K (6 eV and 7 eV) and 200 K (7 eV). The top curve shows the 200 K spectrum divided by the Fermi-Dirac distribution.

measurements were carried out on the same system using a 7 eV vacuum-ultraviolet laser with a repetition rate of 1 GHz, achieving an energy resolution of 0.26 meV with a beam spot size of about 35 μm. Unless otherwise specified, all measurements were performed at 4.5 K. High-quality single crystals of $4H_b$-TaS_2 were grown by chemical vapor transport and cleaved in situ under ultrahigh vacuum prior to measurement.

Equilibrium ARPES spectra near the Brillouin-zone center ($h\nu$ = 7 eV, 4.5 K) reveal a prominent band at approximately −0.5 eV [Fig. 1(b)], a hallmark of the T-terminated surface [22,29]. We also observe pronounced spectral weight with a sharp peak near E_F at Γ, which is confirmed independently at $h\nu$ = 6 eV [Fig. 1(c)]. Because of the distinct work functions of H (6.2 eV) and T terminations (5.7 eV) [29], 6-eV photons selectively probe T-layer terminations. This near-E_F feature is further evidenced by the momentum-integrated EDCs around Γ, which show a resolution-limited peak pinned near E_F at 4.5 K [Fig. 1(d)], consistent with previous reports of a CDW-related near-E_F feature in $4H_b$-TaS_2 [23,29]. This suggests that the relevant band edge resides slightly above E_F at elevated temperature, consistent with nearly complete T-to-H charge transfer [22,24]. To estimate the energy position of the band edge, we divide the 200 K spectrum by the corresponding Fermi-Dirac distribution, revealing a clear peak at ∼0.07 eV. However, the accompanying temperature-dependent chemical-potential shift limits the ability of thermal population alone to reveal the full dispersion [Fig. S8 in the Supplementary Materials (SM)], thereby motivating low-temperature TRARPES measurements.

To access the electronic states above E_F at low temperature, we use TRARPES to track the ultrafast population of normally unoccupied bands (Fig. 2). At 0.05 ps and a pump fluence of 0.8 mJ/cm^2, we observe a narrow feature slightly above E_F, separated by a distinct energy gap from a higher-lying dispersive electron-like band [Fig. 2(a)]. EDC analysis in the minimum-gap region reveals two well-separated peaks. Lorentzian fits at 0 ps yield a band-edge energy of approximately 0.01 eV above E_F and a gap size of approximately 0.26 eV. These observations are broadly consistent with previous calculations and spectroscopy placing a CDW-related near-E_F feature on the T termination [25]; however, the limited momentum coverage of the present measurements does not allow us to determine its full dispersion. As the delay time increases to 0.15 ps, the low-energy feature transiently shifts upward to about 0.06 eV while the gap narrows to approximately 0.17 eV. Beyond 0.2 ps, the upper dispersive feature fades as the photoexcited population relaxes. Upon increasing the

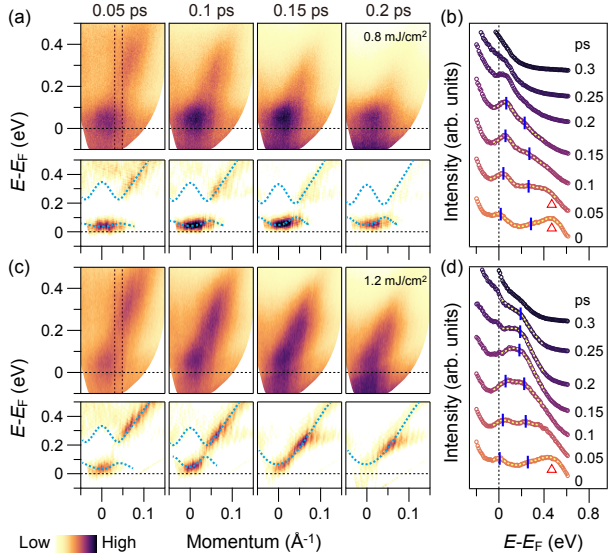

Fig. 2. Ultrafast dynamics and melting of the CDW gap. (a) and (c) Temporal evolution of TRARPES snapshots along the Γ–M direction at 4.5 K, acquired with pump fluences of 0.8 mJ/cm^2 and 1.2 mJ/cm^2, respectively. The top and bottom rows display the raw photoemission intensity and the corresponding curvature spectra. Blue dashed curves highlight the quasiparticle dispersions. Brown vertical lines denote the momentum-integration window around the minimum-gap region. (b) and (d) Corresponding temporal evolution of the momentum-integrated EDCs. Dashed curves are Lorentzian fits, and blue ticks indicate the extracted peak positions. Triangular markers denote the fitted peak positions of the image-potential state, whose contribution is included separately in the multipeak analysis.

pump fluence to 1.2 mJ/cm^2, the gap is nearly closed by 0.15 ps, as evidenced in both the energy-momentum dispersion and the corresponding EDCs [Figs. 2(c) and 2(d)]. The photoinduced gap closing persists beyond 0.3 ps, indicating a pronounced reconstruction of the CDW-gapped electronic structure. Collectively, these results establish a pronounced suppression and near-closing of the resolvable CDW gap, accompanied by a reconstruction of the near-E_F electronic structure.

From Figs. 3(a) and 3(b), we operationally define $F_c \approx 1.4$ mJ/cm^2 as the incident fluence at which the two fitted EDC peaks become unresolved within the fitting uncertainty. Thus, F_c denotes a characteristic crossover rather than a thermodynamic phase boundary. Notably, the mid-gap spectral weight increases with pump fluence, suggesting that the apparent collapse of the CDW gap likely involves both gap filling caused by the loss of CDW coherence and gap shrinkage associated with suppression of the CDW order-parameter amplitude. The less than 10% variation quoted across scans describes relative reproducibility, including pump–probe overlap drift (SM Discussion III).

Above F_c, enhanced occupied-state spectral weight from E_F to approximately −0.2 eV persists for at least 25 ps [Figs. 3(c) and 3(d)]. We operationally term this reconstruction "metastable", although no single observable uniquely identifies a hidden-state analogue. The response saturates above F_c at 0.25 ps but, at 25 ps, recovers below F_c while remaining fluence-dependent above it. Thus, the prompt gap loss and long-delay reconstruction are distinct but potentially connected stages; their similar crossover fluences do not establish causality. This evolution is summarized in the inset of Fig. 3(d).

The ultrafast evolution of the photoinduced spectral weight is analyzed to elucidate the formation of the metastable state (Fig. 4). At low pump fluences, the near-E_F photoemission intensity exhibits pronounced oscillations, which are strongly suppressed as the fluence exceeds F_c [Fig. 4(a)]. Fourier-transform analysis resolves three phonon modes at 1.8, 2.4, and 3.3 THz, in excellent agreement with Raman data [30,31]. The dominant 2.4 THz mode, identified as the A_{1g} CDW amplitude mode of the T layers [32], softens continuously with increasing

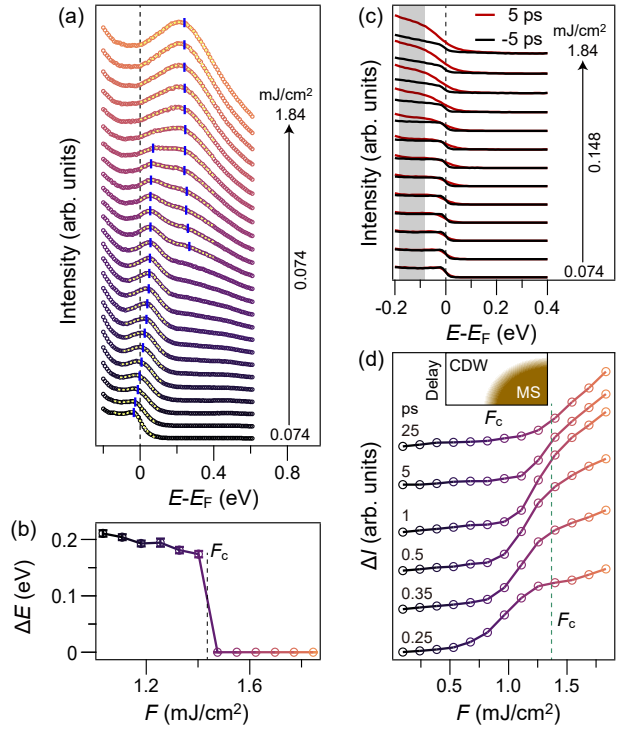

Fig. 3. Fluence-dependent TRARPES spectra at 4.5 K. (a) EDCs at 0.1 ps for various pump fluences, integrated over $k \in [-0.05, 0.1]$ Å^{-1}. Dashed curves represent Lorentzian fits, with blue ticks indicating the extracted peak positions. (b) Extracted gap size ΔE as a function of fluence at 0.1 ps. (c) EDCs at −5 and 5 ps for different fluences. Pump-induced energy shifts were corrected as described in SM Discussion I. (d) Integrated spectral-intensity change ΔI versus fluence for delays from 0.25 to 25 ps. The energy-integration range corresponds to the shaded area in (c). The vertical dashed line indicates the operational characteristic crossover fluence F_c. Corresponding EDCs are shown in SM Fig. S4. The inset is a schematic recovery map, rather than a thermodynamic phase diagram; its graded boundary denotes the crossover into a recovery pathway containing a metastable intermediate state (MS).

fluence, while its linewidth broadens and its amplitude is strongly suppressed [Fig. 4(c); see also SM Discussion II and Fig. S2]. The agreement between common-window Fourier analyses and direct damped-oscillator fits indicates that the downward frequency trend is not solely a windowing artifact. These observations are consistent with a substantial suppression of the coherent CDW response. Concomitantly, a strong enhancement of the occupied-state spectral weight below E_F emerges for $F > F_c$ [Fig. 4(d)], over the same characteristic fluence range as in Fig. 3. While the primary CDW order starts to recover on a picosecond timescale (τ_{fast}), a second, much slower relaxation component becomes prominent. This slow component is evidenced by the kink-like behavior appearing between 5 and 10 ps in the integrated spectral-weight kinetics above F_c, and a two-component exponential fit yields a characteristic lifetime of $\tau_{slow} \approx 50$ ps.

We first consider the mechanism underlying the ultrafast photoinduced collapse of the CDW gap. Our TRARPES measurements of the unoccupied states (Fig. 2) indicate that the CDW opens a gap that leaves a weakly dispersive band-edge feature near E_F at the bottom of an electron-like dispersion. Upon photoexcitation, the resolvable gap is lost on a timescale comparable to our 113-fs temporal resolution, a timescale comparable to one-quarter of the A_{1g} CDW amplitude-mode period. This rapid response is characteristic of a displacive excitation mechanism, in which photoexcitation transiently shifts the lattice equilibrium position from the CDW-distorted configuration toward the high-symmetry structure. This process reflects a transient rectification of the potential energy surface, effectively melting the CDW order before the lattice can complete a full vibrational cycle [33,34]. Such ultrafast dynamics are consistent with electron-phonon-coupling-driven CDW formation observed in bulk 1T-TaS_2 [16,35,36], suggesting that the fundamental mechanism of CDW stabilization within individual T layers remains robust in the 4H_b-TaS_2 heterostructure.

Next we discuss possible microscopic interpretations of the photoinduced metastable state. As described above, it is defined operationally by a persistent enhancement of the occupied spectral weight below E_F during recovery, after the short-lived unoccupied carrier population has decayed. Once the excitation exceeds F_c, the recovery develops fast and slow components. In bulk 1T-TaS_2, optical or electrical melting of the CDW can drive the system into a hidden metallic state with an extremely long lifetime at low temperature [19,21,37]. In 4H_b-TaS_2, the long-delay occupied-state enhancement and slow recovery resemble aspects of the bulk hidden-state response, but the present ARPES data do not uniquely establish an identical microscopic state or a particular real-space domain structure. Within a domain-based interpretation, the fast component may reflect recovery of the CDW order-parameter amplitude and local correlations, while the slow component is consistent with later recovery of long-range phase coherence [38]. Domain walls can provide low-energy spectral weight in bulk 1T-TaS_2 [39,40], but their presence here is not directly imaged.

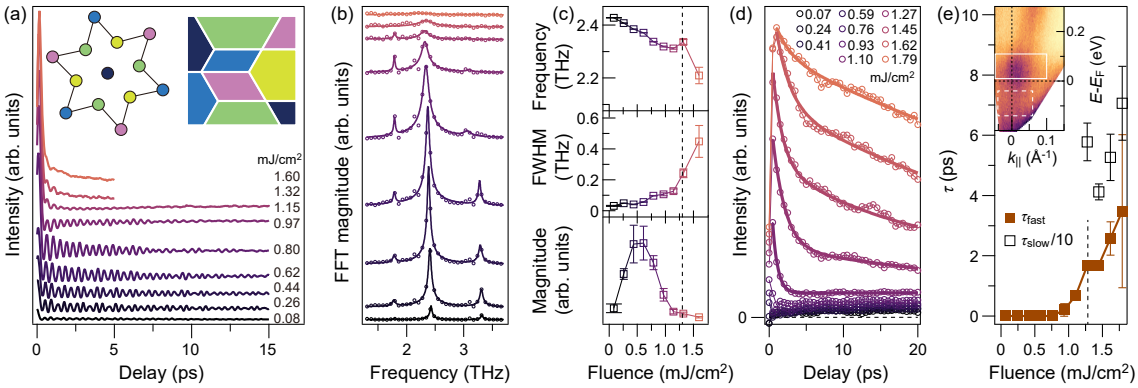

Fig. 4. Fluence-dependent dynamics of the CDW amplitude mode and metastable state. (a) Temporal evolution of the band-edge intensity at various pump fluences. Data represent the spectral weight integrated over the window defined by the solid box in the inset of (e). Insets: (left) schematic of the SOD cluster with color-coded Ta sites; (right) schematic of CDW domains with distinct phases (SM Fig. S5). (b) Magnitude of the Fourier transforms of the curves in (a) after subtraction of a smooth background. Solid curves are Lorentzian fits. (c) Pump-fluence dependence of the frequency, full width at half maximum (FWHM), and amplitude of the 2.4 THz A_{1g} amplitude mode, extracted from Lorentzian fits to the Fourier spectra. (d) Temporal evolution of the integrated spectral weight within the dashed box shown in the inset of (e). Solid curves represent single-component fits below F_c and two-component fits above F_c. Oscillations are not resolved in panel (d) because the data were acquired with a delay step of 0.5 ps. (e) Extracted relaxation timescales τ_{fast} and τ_{slow} as a function of pump fluence. For clarity, τ_{slow} is divided by 10. Inset: TRARPES spectrum at $t = 0.05$ ps ($F = 0.8$ mJ/cm^2).

A complementary possible pathway is mode-selective phonon thermalization. Energy transferred preferentially to strongly coupled phonons can remain out of equilibrium after the hot-carrier population has decayed and may hinder the re-establishment of long-range phase coherence [41,42].

Nevertheless, a crucial distinction from bulk 1T-TaS_2 is that the metastable state in $4H_b$-TaS_2 has a characteristic slow relaxation time of about 50 ps. A possible alternative explanation for this difference is cumulative heating associated with the high repetition rate used in our measurements, which could accelerate the recovery of the hidden state [43]. Using the same experimental platform, base temperature, and repetition rate, but a different write–read protocol and the preparation fluence specified in SM Fig. S10, we generated a bulk 1T-TaS_2 hidden state that persisted without detectable change over the subsequent ARPES measurement. This benchmark disfavors the repetition rate or cumulative heating as the sole explanation for the sub-100-ps lifetime in $4H_b$-TaS_2, but it is not a fully matched dynamical control. In bulk 1T-TaS_2, formation of the hidden state is accompanied by a pronounced reconstruction of the out-of-plane CDW stacking and the collapse of interlayer dimerization [20,44]. The intervening H layers in $4H_b$-TaS_2 interrupt direct T–T stacking and may inhibit a stacking rearrangement of the type associated with the bulk hidden state. We therefore regard reduced direct interlayer coupling as one plausible contribution to the shorter lifetime, rather than as a uniquely established mechanism. Electronic and phononic contributions from the neighboring H layers cannot be excluded. After SPV correction, the absence of an additional rigid T-layer band shift disfavors a large transient charge-transfer response but not subtler screening, hybridization, or relaxation channels. Although distinct two-dimensional CDWs occur in the T and H/H′ layers [45], our measurements cannot separate their structural and electronic contributions. Possible effects on superconductivity, measured here above T_c, await lower-temperature studies.

In summary, our TRARPES study clarifies the ultrafast evolution of the CDW-gapped electronic structure on the T termination of $4H_b$-TaS_2. Above a characteristic fluence, the resolvable CDW gap is lost and an occupied-state reconstruction persists for tens of picoseconds after hot carriers decay, identifying a transient metastable electronic state without implying microscopic identity with the persistent bulk 1T-TaS_2 hidden state. Although the excitation conditions are not fully matched, the lifetime contrast is consistent with a role for interrupted direct T–T stacking, while H-layer relaxation channels remain unresolved. Our results establish ultrafast optical excitation as a powerful means to control correlated states and emergent phenomena in layered quantum heterostructures.

Acknowledgements

W. T. Z. acknowledges support from the National Key R&D Program of China (Grant Nos. 2021YFA1400202 and 2021YFA1401800), the National Natural Science Foundation of China (Grant No. 12525404), and the Natural Science Foundation of Shanghai (Grant Nos. 22ZR1479700 and 23XD1422200). H. C. L. acknowledges support from the National Key R&D Program of China (Grant Nos. 2023YFA1406500 and 2022YFA1403800) and the National Natural Science Foundation of China (Grant No. 12274459). S. F. D. acknowledges support from the National Natural Science Foundation of China (Grant No. 12304178). D. Q. acknowledges support from the National Key R&D Program of China (Grant Nos. 2022YFA1402400 and 2021YFA1400100) and the National Natural Science Foundation of China (Grant No. 12074248).

References

[1] de la Torre A, Kennes D M, Claassen M, Gerber S, McIver J W, and Sentef M A 2021 *Rev. Mod. Phys.* **93** 041002
[2] Bao C, Tang P, Sun D, and Zhou S 2021 *Nat. Rev. Phys.* **4** 33
[3] Novoselov K S, Mishchenko A, Carvalho A, and Castro Neto A H 2016 *Science* **353** aac9439
[4] Žutić I, Matos-Abiague A, Scharf B, Dery H, and Belashchenko K 2019 *Mater. Today* **22** 85
[5] Yang Y, Fang S, Fatemi V, Ruhman J, Navarro-Moratalla E, Watanabe K, Taniguchi T, Kaxiras E, and Jarillo-Herrero P 2018 *Phys. Rev. B* **98** 035203
[6] Chen H, Wang F H, Gao Q, Gao X J, Chen Z, Huang Y, Law K T, Xu X Y, and Chen P 2025 *Phys. Rev. Lett.* **134** 066402
[7] Di Salvo F, Bagley B, Voorhoeve J, and Waszczak J 1973 *J. Phys. Chem. Solids* **34** 1357
[8] Kim J J and Olin H 1995 *Phys. Rev. B* **52** R14388
[9] Ekvall I, Kim J J, and Olin H 1997 *Phys. Rev. B* **55** 6758
[10] Wang H, Jiao Y, Meng F, Zhang X, Dai D, Tu C, Zhao C, Xin L, Huang S, Lei H, and Li S 2025 *Phys. Rev. Lett.* **135** 126002
[11] Ribak A, Skiff R M, Mograbi M, Rout P K, Fischer M H, Ruhman J, Chashka K, Dagan Y, and Kanigel A 2020 *Sci. Adv.* **6** eaax9480
[12] Nayak A K, Steinbok A, Roet Y, Koo J, Margalit G, Feldman I, Almoalem A, Kanigel A, Fiete G A, Yan B, Oreg Y, Avraham N, and Beidenkopf H 2021 *Nat. Phys.* **17** 1413
[13] Persky E, Bjørlig A V, Feldman I, Almoalem A, Altman E, Berg E, Kimchi I, Ruhman J, Kanigel A, and Kalisky B 2022 *Nature* **607** 692
[14] Zhou Y, Meng F, Huang Y, Zhang J, Zhan J, Chen Y, Liu Y, Lei H, Smidman M, and Yuan H 2025 *Phys. Rev. B* **112** 014507
[15] Wu P, Wang Z, Zhang Y, Chen Z, Yu S, Ma W, Shan M, Liang Z, Wei X, Wang J, Cheng W, Liang Z, Zhang X, Wu T, Okada Y, Jiang K, Wang Z, and Chen X 2025 arXiv: 2508.17861 [cond-mat.supr-con]
[16] Rossnagel K 2011 *J. Phys.: Condens. Matter* **23** 213001
[17] Law K T and Lee P A 2017 *Proc. Natl. Acad. Sci. USA* **114** 6996
[18] Lee S H, Goh J S, and Cho D 2019 *Phys. Rev. Lett.* **122** 106404
[19] Stojchevska L, Vaskivskyi I, Mertelj T, Kusar P, Svetin D, Brazovskii S, and Mihailovic D 2014 *Science* **344** 177
[20] Stahl Q, Kusch M, Heinsch F, Garbarino G, Kretzschmar N, Hanff K, Rossnagel K, Geck J, and Ritschel T 2020 *Nat. Commun.* **11** 1247
[21] Ma L, Ye C, Yu Y, Lu X F, Niu X, Kim S, Feng D, Tománek D, Son Y W, Chen X H, and Zhang Y 2016 *Nat. Commun.* **7** 10956
[22] Almoalem A, Gofman R, Nitzav Y, Mangel I, Feldman I, Koo J, Mazzola F, Fujii J, Vobornik I, Sánchez-Barriga J, Clark O J, Plumb N C, Shi M, Yan B, and Kanigel A 2024 *npj Quantum Mater.* **9** 36
[23] Yang F Z, Zhang H D, Mandal S, Meng F Y, Fabbris G, Said A H, Mercado Lozano P, Rajapitamahuni A, Vescovo E, Nelson C, Lin S, Park Y, Clements E M, Ward T Z, Lee H N, Lei H C, Liu C X, and Miao H 2025 *Nat. Commun.* **16** 6626
[24] Crippa L, Bae H, Wunderlich P, Mazin I I, Yan B, Sangiovanni G, Wehling T, and Valentí R 2024 *Nat. Commun.* **15** 1357
[25] Kumar Nayak A, Steinbok A, Roet Y, Koo J, Feldman I, Almoalem A, Kanigel A, Yan B, Rosch A, Avraham N, and Beidenkopf H 2023 *Proc. Natl. Acad. Sci. USA* **120** e2304274120
[26] Yang W, Karbasizadeh S, Jeon H, Hus S, Baddorf A P, Mu S, Berlijn T, Zhou H, Ko W, and Li A P 2025 *Phys. Rev. B* **112** 245126
[27] Yang Y, Tang T, Duan S, Zhou C, Hao D, and Zhang W 2019 *Rev. Sci. Instrum.* **90** 063905
[28] Huang C, Duan S, and Zhang W 2022 *Quantum Front.* **1** 15
[29] Date M, Bae H, Louat A, Domaine G, Schröter N B M, Como E D, Yan B, and Watson M D 2026 *Commun. Phys.* **9** 61
[30] Nakashizu T, Sekine T, Uchinokura K, and Matsuura E 1984 *Phys. Rev. B* **29** 3090
[31] Bang J, Lee B, Yang H, Kim S, Wulferding D, and Cho D 2024 *Phys. Rev. B* **109** 195170
[32] Maklar J, Sarkar J, Dong S, Gerasimenko Y A, Pincelli T, Beaulieu S, Kirchmann P S, Sobota J A, Yang S, Leuenberger D, Moore R G, Shen Z X, Wolf M, Mihailovic D, Ernstorfer R, and Rettig L 2023 *Sci. Adv.* **9** eadi4661
[33] Schmitt F, Kirchmann P S, Bovensiepen U, Moore R G, Rettig L, Krenz M, Chu J H, Ru N, Perfetti L, Lu D H, Wolf M, Fisher I R, and Shen Z X 2008 *Science* **321** 1649
[34] Zeiger H J, Vidal J, Cheng T K, Ippen E P, Dresselhaus G, and Dresselhaus M S 1992 *Phys. Rev. B* **45** 768
[35] Liu A Y 2009 *Phys. Rev. B* **79** 220515
[36] Hellmann S, Rohwer T, Kalläne M, Hanff K, Sohrt C, Stange A, Carr A, Murnane M, Kapteyn H, Kipp L, Bauer M, and Rossnagel K 2012 *Nat. Commun.* **3** 1069
[37] Gao F Y, Zhang Z, Sun Z, Ye L, Cheng Y H, Liu Z J, Checkelsky J G, Baldini E, and Nelson K A 2022 *Sci. Adv.* **8** eabp9076

[38] Vogelgesang S, Storeck G, Horstmann J G, Diekmann T, Sivis M, Schramm S, Rossnagel K, Schäfer S, and Ropers C 2017 *Nat. Phys.* **14** 184

[39] Cho D, Cheon S, Kim K S, Lee S H, Cho Y H, Cheong S W, and Yeom H W 2016 *Nat. Commun.* **7** 10453

[40] Huber M, Zuber S, Rosa-Rocha V, Haley S C, Dale N, Moreschini L, Lee D H, Bostwick A, Jozwiak C, Analytis J G, and Lanzara A 2025 *Commun. Phys.* **8** 469

[41] Kurtz F, Dauwe T N, Yalunin S V, Storeck G, Horstmann J G, Böckmann H, and Ropers C 2024 *Nat. Mater.* **23** 890

[42] Cheng Y, Zong A, Wu L, Meng Q, Xia W, Qi F, Zhu P, Zou X, Jiang T, Guo Y, Van Wezel J, Kogar A, Zuerch M W, Zhang J, Zhu Y, and Xiang D 2024 *Nat. Phys.* **20** 54

[43] Vaskivskyi I, Gospodaric J, Brazovskii S, Svetin D, Sutar P, Goreshnik E, Mihailovic I A, Mertelj T, and Mihailovic D 2015 *Sci. Adv.* **1** e1500168

[44] Zhang J, Yang Y, Zhang J, Guan M, Xu J, Yang K, Shi X, and Meng S 2025 arXiv: 2502.17985 [cond-mat.mtrl-sci]

[45] Yang F Z, Zhang T T, Meng F Y, Lei H C, Nelson C, Cai Y Q, Vescovo E, Said A H, Lozano P M, Fabbris G, and Miao H 2025 *Phys. Rev. B* **111** L041101